Transition-State Spectroscopy of Cyclooctatetraene

Paul G. Wenthold, David A. Hrovat, Weston Thatcher Borden,* W. Carl Lineberger*

The 351-nanometer photoelectron spectrum of the planar cyclooctatetraene radical anion ($COT^{\cdot-}$) shows transitions to two electronic states of cyclooctatetraene (COT). These states correspond to the D_{4h} $^1A_{1g}$ state, which is the transition state for COT ring inversion, and the D_{8h} $^3A_{2u}$ state. The electron binding energy of the $^1A_{1g}$ transition state is 1.099 ± 0.010 electron volts, which is lower by 12.1 ± 0.3 kilocalories per mole than that of the $^3A_{2u}$ state. The photoelectron spectrum shows that the singlet lies well below the triplet in D_{8h} COT and confirms ab initio predictions that the molecule violates Hund's rule. Vibrational structure is observed for both features and is readily assigned by use of a simple potential energy surface.

We report a photodetachment study of the planar cyclooctatetraene radical anion ($COT^{\cdot-}$) and the direct observation of the planar transition state for the ring inversion of cyclooctatetraene (COT). Detailed structural and energetic information on the planar transition state for the ring inversion of COT was obtained. This is by far the most complex system for which detailed structural information on a transition state has been experimentally accessible. Our results show that planar, octagonal (D_{8h}) COT has a singlet ground state and thus violates Hund's rule.

Until recently, studies of transition states for chemical reactions were carried out indirectly, with the nature of the state inferred from observation of reaction kinetics, isotope and substituent effects, and the stereochemical outcome. Advances in laser technology and spectroscopic techniques have made it possible in certain cases to observe and study transition regions directly (*1*). Basically, two techniques have been developed for the investigation of transition-state properties. The first involves capturing a bimolecular scattering event in the brief moment during which the reactants pass through the transition region. The second involves the use of either a group of atoms or an electron to fix a complex at a geometry that corresponds to a transition state when the stabilizing feature is removed.

The first examples of transition-state spectroscopy involved the study of metal halide exchange reactions in molecular beam experiments (*2*). The signatures of transition states were minor in such experiments, and, at present, most transition-state studies use a departing group or electron. Zewail and co-workers have used photochemical deiodination and decarbonylation to investigate in real-time concertedness in elimination reactions (*3*) and the nature of tri- and tetramethylene diradicals (*4*), respectively. The primary difficulty with such measurements is that the departing group may still be associated with the complex during the reaction, which complicates the interpretation of these experiments.

In contrast, when a transition state is accessed by removal of an electron, the nuclei are essentially frozen during the time that the electron is in the neighborhood of the complex. For example, photodetachment of FH_2^- leads to formation of FH_2 at a geometry near the transition state for the reaction of F + H_2 (*5*). Using this technique, Neumark has carried out vibrationally resolved transition-state spectroscopy of small systems (*6*). Indeed, photodetachment provides a general means for accessing electronic states and regions of potential energy surfaces that cannot be readily studied by other spectroscopic techniques (*7*). However, all of the previous transition-state spectroscopy based on the use of this technique and those described above have been restricted to relatively small, simple systems. We now show that it is possible to extend the photodetachment technique to the investigation of the transition state for ring inversion in COT, a large molecule whose electronic structure at planar geometries is of considerable interest.

Planar octagonal (D_{8h}) COT has a degenerate (e_{2u}) pair of nonbonding molecular orbitals (NBMOs) that are occupied by two electrons. Therefore, Hund's rule (*8*) predicts that COT should have a triplet ground state ($^3A_{2u}$). However, the two e_{2u} NBMOs of COT can be chosen so that they have no atoms in common, and qualitative theory (*9*) predicts that biradicals with disjoint NBMOs will have singlet ground states. Electronic structure calculations (*10*, *11*) provide computational support for the qualitative prediction that D_{8h} COT will have a singlet ground state ($^1B_{1g}$) and therefore will violate Hund's rule.

Violations of Hund's rule have been predicted (*12*) and found (*13*) in tetramethylenebenzene and in other molecules (*14*) that may be considered to be derivatives of disjoint, non-Kekulé, hydrocarbon diradicals. However, the NBMOs in these non-Kekulé diradicals do not have exactly the same energy, and this nondegeneracy contributes to making the singlet the ground state (*14*). Consequently, it can be argued that the singlet ground states found for these disjoint diradicals do not constitute violations of the strictest form of Hund's rule.

In contrast to the NBMOs in the non-Kekulé diradicals, the e_{2u} NBMOs of D_{8h} COT are degenerate by symmetry. The greater electron correlation in the singlet—a consequence of the nonuniform distribution of electron spins that results from the presence of an alpha spin electron in one disjointed NBMO and a beta spin electron in the other (*9*)—is wholly responsible for the predicted singlet ground state of D_{8h} COT. Confirmation that D_{8h} COT does, in fact, have a singlet ground state is of con-

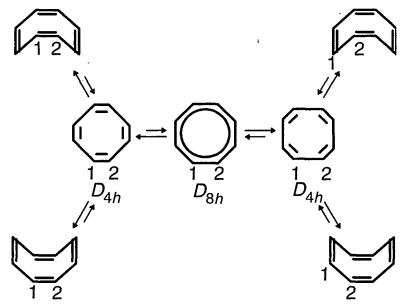

Fig. 1 (left). Ring inversion and bond shifting processes in COT. **Fig. 2 (right).** Photoelectron spectrum of the cyclooctatetraene radical anion ($COT^{\cdot-}$) (351 nm).

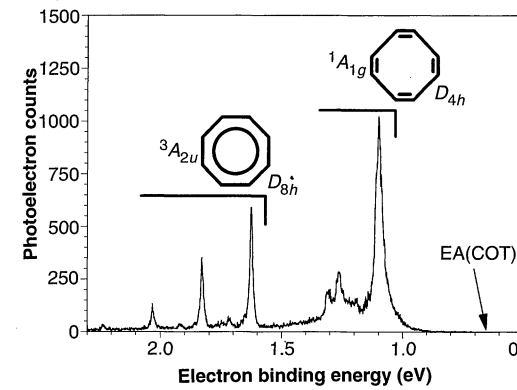

P. G. Wenthold and W. C. Lineberger, JILA and Department of Chemistry and Biochemistry, University of Colorado, and National Institute of Standards and Technology, Boulder, CO 80309, USA.
D. A. Hrovat and W. T. Borden, Department of Chemistry, Box 351700, University of Washington, Seattle, WA 98195, USA.
*To whom correspondence should be addressed.

siderable importance because it would provide experimental evidence that violations of Hund's rule actually do occur in disjoint diradicals, even when the NBMOs are strictly degenerate.

Experimental verification that D_{8h} COT has a singlet ground state is challenging. Triplet COT is predicted to have a D_{8h} equilibrium geometry (*10*, *11*), but earlier attempts to use electron paramagnetic resonance (EPR) to observe this state during triplet-sensitized photolysis of COT (*14*) or by photodetachment of an electron from $COT^{\cdot-}$ (*15*) have failed. The main challenge in showing experimentally that singlet COT is lower in energy than the triplet at planar, octagonal (D_{8h}) geometries lies in the fact that the equilibrium geometry of the lowest energy singlet state is nonplanar with alternating single and double carbon-to-carbon bonds (*16*). Elegant dynamic nuclear magnetic resonance (NMR) experiments, albeit on derivatives of COT, indicate that ring inversion of the D_{2d} equilibrium geometry of COT has an activation energy of 10 to 11 kcal mol^{-1} and that bond shifting in COT requires an additional 3 to 4 kcal mol^{-1} (Fig. 1) (*17*–*19*).

The proposal of Anet *et al.* (*18*) that the transition state for ring inversion is planar with alternating single and double carbon-to-carbon bonds (D_{4h} symmetry) seems to have been generally accepted (*16*, *19*) and is supported by the results of ab initio calculations (*10*). The D_{4h} structure results from second-order Jahn-Teller distortion in COT, which splits the e_{2u} orbitals into nondegenerate b_{1u} and b_{2u} orbitals. Although nonplanar transition-state geometries have been proposed for bond shifting in singlet COT (*20*), multiconfiguration self-consistent field (MCSCF) calculations (*10*) support Anet's earlier supposition (*17*, *18*) that the transition state for bond shifting in unsubstituted COT is planar with D_{8h} symmetry. A bond-shifting transition state of lower symmetry cannot be rigorously excluded, but a careful search at the MCSCF(8,8)/6-31G* level of theory (*10*) for such a transition state failed to find one, and the calculated barriers to both bond shifting and ring inversion are in excellent agreement with the values from the NMR experiments (*17*–*19*).

Photodetachment spectroscopy of $COT^{\cdot-}$ provides a promising means both for observing the D_{4h} and D_{8h} transition states for singlet COT and the lowest D_{8h} triplet state and for measuring their relative energies. Previous EPR (*21*), NMR (*22*), and ultraviolet-visible spectroscopy (*15*, *23*) studies all indicate that $COT^{\cdot-}$ has a planar geometry in solution, and ab initio calculations indicate a bond-alternated, D_{4h} geometry in the gas phase as well (*24*). The tremendous structural difference between the planar D_{4h} equilibrium geometry of $COT^{\cdot-}$ and the nonplanar D_{2d} geometry of ground-state COT should render transitions from the former to the latter too weak to be observed at energies near the electron affinity (EA), but transitions to planar geometries of the singlet and triplet states of COT are expected to be strong.

In 1979, Brauman and co-workers (*25*) reported the photodetachment spectrum of $COT^{\cdot-}$. The cross section for photodetachment increased slowly above the energy at which photodetachment was first detected (0.8 ± 0.1 eV), but they did not detect features attributable either to excited vibrational states or to the onset of a second electronic state. The apparent photodetachment threshold energy was well above the adiabatic EA of COT (~0.6 eV), which was previously estimated from thermal electron capture kinetics (*26*). However, in molecules such as COT where there is a large geometry change between the anion and neutral, accurate determination of the adiabatic EA is difficult for both spectroscopic and kinetic methods (*27*).

Electron capture by COT in a flowing afterglow ion source cooled with liquid nitrogen formed the $COT^{\cdot-}$ ions. The 351-nm photoelectron spectrum of $COT^{\cdot-}$, obtained with the negative-ion photoelectron spectrometer and experimental protocol described in (*7*), is shown in Fig. 2. No photoelectrons were observed at electron binding energies near 0.6 eV, the expected EA of COT. However, photodetachment to two distinct electronic states of COT was observed in the spectrum. The lower binding energy feature corresponds to transitions to one electronic state, the intense, asymmetric peak being the origin (1.099 ± 0.010 eV binding energy) and the three weaker peaks (740 ± 60, 1315 ± 40, and 1670 ± 40 cm^{-1}) corresponding to excited vibrational levels. This feature corresponds to formation of the $^1A_{1g}$ state of D_{4h} COT.

The feature at higher binding energy is composed of a vibrational progression with an origin at 1.624 ± 0.006 eV. The vibrations are at 1635 ± 20 cm^{-1} (strong) and at 735 ± 20 cm^{-1} (weaker). The intensities of the peaks that correspond to the higher frequency vibration indicate a large geometry change along the coordinate for this vibrational mode on going from the equilibrium geometry of $COT^{\cdot-}$ to that of this upper energy state. We assign this state as $^3A_{2u}$ of D_{8h} COT. This method of generating triplet COT from $COT^{\cdot-}$ in the gas phase is analogous to that of Dvorak and Michl (*15*), who attempted to observe the $^3A_{2u}$ state upon photodetachment of matrix-isolated $COT^{\cdot-}$.

The photoelectron spectrum of $COT^{\cdot-}$ can be understood in terms of the schematic diagrams shown in Figs. 3 and 4. The potential energy surfaces for planar COT are shown in Fig. 3. The *x* axis for the potential energy surfaces in Fig. 3 is the bond-alternation coordinate, which connects the two different D_{4h} geometries through a D_{8h} geometry, where all the C–C bond lengths are equal. The dotted curve, shown for $^1A_{1g}$, corresponds to the potential energy along the coordinate for ring inversion, orthogonal to the coordinate for bond alternation. The molecular orbitals for the planar states of COT and their orbital occupancies are shown in Fig. 4. Both the lowest energy

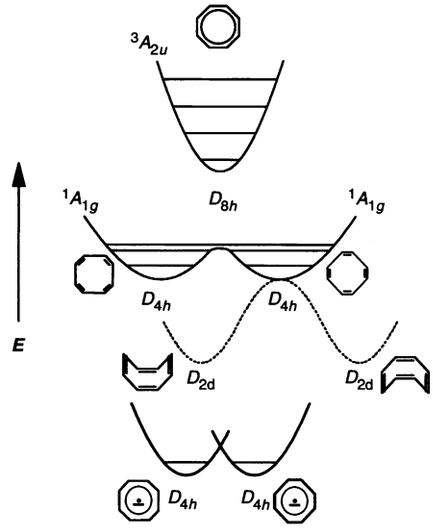

Fig. 3. Schematic potential energy surfaces for $COT^{\cdot-}$ and for singlet and triplet COT. The *x* axis is the "bond-alternation" coordinate for the planar molecule. The *z* axis is the out-of-plane bending coordinate, and the potential energy curves for this coordinate are shown with dotted lines.

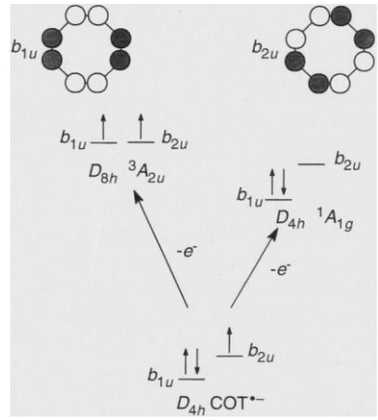

Fig. 4. Top view of the pair of MOs that are occupied in $COT^{\cdot-}$ and planar COT. The greater occupancy of the b_{1u} MO in $COT^{\cdot-}$ and in the $^1A_{1g}$ state of COT causes these two states to "prefer" bond-alternated, D_{4h} geometries, whereas the triplet state "prefers" a geometry where the C–C bond lengths are equal and the b_{1u} and b_{2u} orbitals are degenerate.

singlet and triplet surfaces can be accessed upon photodetachment of the D_{4h} $^2B_{2u}$ ion.

It is easiest to analyze the spectrum in Fig. 2 by first considering the higher energy feature, which we assign to the formation of triplet COT. The stronger vibrational progression observed for this state corresponds to the bond alternation vibrational mode of the $^3A_{2u}$ state of D_{8h} COT. This mode is activated upon detachment of D_{4h} COT because the equilibrium geometries of $COT^{\cdot-}$ and triplet COT differ along this coordinate (Fig. 3). The differences in the geometries of these species allow the wave function for the lowest vibrational state of $COT^{\cdot-}$ to have significant Franck-Condon overlap with the wave functions for four of the vibrational levels of the $^3A_{2u}$ state of COT.

The observed 1635-cm^{-1} vibrational frequency agrees well with the value of 1615 cm^{-1} that was calculated for this mode by the scaling of the MCSCF(8,8)/6-31G* harmonic frequency by 0.91 to account for anharmonicity and dynamic correlation effects (*28*). The weaker 735 cm^{-1} progression is assigned to the symmetric ring-breathing mode, which is calculated to be 713 cm^{-1}. Not only the positions but also the intensities of the vibrational peaks of the higher energy feature in Fig. 2 are in excellent agreement with those obtained from the use of a modeling procedure (*29*), in which the Franck-Condon factors were calculated from the MCSCF(8,8)/6-31G* geometries and frequencies for $COT^{\cdot-}$ and for the $^3A_{2u}$ state of COT.

The lower energy feature in the spectrum is assigned to formation of the $^1A_{1g}$ state of D_{4h} COT, the transition state for ring inversion. Although this geometry is a saddle point on the singlet potential energy surface, the imaginary frequency at this geometry is computed to be small ($90i$ cm^{-1}), indicating that the surface is relatively flat in this region. Therefore, the peaks in the spectrum are not excessively broadened (full width at half maximum $\approx$ 0.05 eV) (*6*).

The first excited vibration at 740 cm^{-1} can be assigned to the ring-breathing mode, which is calculated to be nearly the same in $^1A_{1g}$ and $^3A_{2u}$. However, the intense series of vibrational peaks in the band for $^3A_{2u}$, assigned to the bond alternation mode, are not seen in the band for $^1A_{1g}$. Instead, we observe a pair of comparatively weak peaks at 1315 and 1670 cm^{-1}.

The scaled MCSCF(8,8)/6-31G* harmonic vibrational frequency calculated for the bond-alternation mode of the $^1A_{1g}$ state is 1535 cm^{-1}. However, at 1535 cm^{-1} (4.4 kcal mol^{-1}), the first excited vibrational level of this mode is expected to be near the top of the barrier at the D_{8h} transition state for interconversion of the two D_{4h} geometries (*10, 17–19*). Thus, as shown schematically in Fig. 3, the in-phase and out-of-phase combinations of the D_{4h} vibrational wave functions should be split by an observable amount, and the observed vibrational frequencies of 1315 and 1670 cm^{-1} are assigned to the symmetric and antisymmetric combinations, respectively.

As suggested in Fig. 3, bond alternation is calculated to be slightly greater in the $^1A_{1g}$ state of COT than in $COT^{\cdot-}$. Therefore, on formation of the $^1A_{1g}$ state of COT from $COT^{\cdot-}$, some vibrational activity in the bond alternation mode is expected. However, because the D_{4h} geometry of $^1A_{1g}$ is somewhat closer to the D_{4h} equilibrium geometry of $COT^{\cdot-}$ than is the D_{8h} geometry of $^3A_{2u}$, the peak intensities for transitions from the lowest vibrational level of $COT^{\cdot-}$ to excited vibrational levels of COT are smaller in $^1A_{1g}$ than in $^3A_{2u}$.

The electron binding energy of the $^1A_{1g}$ state of COT (1.099 $\pm$ 0.010 eV) is $\sim$0.5 eV greater than the reported $\sim$0.6 eV EA of the equilibrium geometry of D_{2d} COT (*26*). The difference between the electron binding energy of singlet D_{4h} COT and the adiabatic EA of singlet D_{2d} COT is equal to the energy difference between the lowest singlet state at these two geometries. Because the D_{4h} $^1A_{1g}$ state of COT is the transition state for ring inversion, the adiabatic EA of COT can be obtained by subtracting the barrier to ring inversion from the $^1A_{1g}$ electron binding energy. The barrier height is estimated to be 10 to 11 kcal mol^{-1} (0.43 to 0.48 eV), both by dynamic NMR studies of monosubstituted derivatives of COT (*18, 19*) and by MCSCF(8,8)/6-31G* calculations on COT itself (*10*). Thus, we find EA(COT) = 0.65 eV, which is close to the estimate of Wentworth and Ristau (*26*).

The singlet-triplet energy splitting in D_{8h} COT can be obtained directly from the photoelectron spectrum. The origin of the triplet state is 0.525 $\pm$ 0.012 eV (12.1 $\pm$ 0.3 kcal mol^{-1}) above the lowest energy planar (D_{4h}) singlet state, and the dynamic NMR studies place the (D_{8h}) transition state for bond shifting in singlet COT 3 to 4 kcal mol^{-1} higher in energy than the (D_{4h}) transition state for ring inversion (*17–19*). Combining these values, we estimate that the D_{8h} singlet state of COT lies 8 to 9 kcal mol^{-1} below the D_{8h} triplet.

Our best computational estimate of this energy difference, based on calculations that go beyond the MCSCF level and include dynamic electron correlation, is $\sim$10 kcal mol^{-1} (*30*). Thus, in addition to predicting qualitatively the violation of Hund's rule in D_{8h} COT (*10*), which our photodetachment spectrum of $COT^{\cdot-}$ confirms, ab initio calculations provide an accurate value of the energy by which the D_{8h} singlet transition state for bond shifting lies below the D_{8h} equilibrium geometry of the triplet in COT.

REFERENCES AND NOTES

1. J. C. Polanyi and A. H. Zewail, *Acc. Chem. Res.* **28**, 119 (1995).
2. P. Arrowsmith *et al.*, *J. Chem. Phys.* **73**, 5895 (1980); P. Arrowsmith, S. H. P. Bly, P. E. Charters, J. C. Polanyi, *ibid.* **79**, 283 (1983); P. R. Brooks, R. F. Curl, T. C. Maguire, *Ber. Bunsenges. Phys. Chem.* **86**, 401 (1982); P. Hering, P. R. Brooks, R. F. Curl Jr., R. S. Judson, R. S. Lowe, *Phys. Rev. Lett.* **44**, 687 (1980); P. R. Brooks, *Chem. Rev.* **88**, 407 (1988).
3. A. H. Zewail, *Femtochemistry—Ultrafast Dynamics of the Chemical Bond* (World Scientific, Teaneck, NJ, 1994).
4. S. Pedersen, J. L. Perek, A. H. Zewail, *Science* **266**, 1359 (1994).
5. D. E. Manolopoulos *et al.*, *ibid.* **262**, 1852 (1993).
6. D. M. Neumark, *Acc. Chem. Res.* **26**, 33 (1993).
7. K. M. Ervin and W. C. Lineberger, in *Advances in Gas Phase Ion Chemistry*, N. G. Adams and L. M. Babcock, Eds. (JAI Press, Greenwich, CT, 1992), vol. 1, pp. 121–166; S. M. Burnett, A. E. Stevens, C. S. Feigerle, W. C. Lineberger, *Chem. Phys. Lett.* **100**, 124 (1983).
8. F. Hund, *Linienspektren Periodisches System der Elemente* (Springer-Verlag, Berlin, 1927); *Z. Phys.* **51**, 759 (1928).
9. W. T. Borden and E. R. Davidson, *J. Am. Chem. Soc.* **99**, 4587 (1977); W. T. Borden, in *Diradicals*, W. T. Borden, Ed. (Wiley-Interscience, New York, 1982), pp. 1–72; *Mol. Cryst. Liq. Cryst.* **232**, 195 (1993).
10. D. A. Hrovat and W. T. Borden, *J. Am. Chem. Soc.* **114**, 5879 (1992).
11. M. J. S. Dewar and K. M. Merz, *J. Phys. Chem.* **89**, 4739 (1985).
12. P. M. Lahti, A. S. Ichimura, J. A. Berson, *J. Org. Chem.* **54**, 958 (1989); P. M. Lahti, A. Rossi, J. A. Berson, *J. Am. Chem. Soc.* **107**, 4362 (1985); P. Du *et al.*, *ibid.* **108**, 5072 (1986); D. A. Hrovat and W. T. Borden, *ibid.* **116**, 6327 (1994).
13. J. H. Reynolds *et al.*, *J. Am. Chem. Soc.* **114**, 763 (1992); J. H. Reynolds, J. A. Berson, J. C. Scaiano, A. B. Berinstain, *ibid.*, p. 5866; J. H. Reynolds *et al.*, *ibid.* **115**, 8073 (1993).
14. W. T. Borden, H. Iwamura, J. A. Berson, *Acc. Chem. Res.* **27**, 109 (1994).
15. V. Dvorak and J. Michl, *J. Am. Chem. Soc.* **98**, 1080 (1976).
16. L. A. Paquette, *Tetrahedron* **31**, 2855 (1975); G. I. Fray and R. G. Saxton, *The Chemistry of Cyclooctatetraene and Its Derivatives* (Cambridge Univ. Press, New York, 1978); L. A. Paquette, *Pure Appl. Chem.* **54**, 987 (1982); *Acc. Chem. Res.* **25**, 57 (1992).
17. F. A. L. Anet, *J. Am. Chem. Soc.* **84**, 671 (1962).
18. _____, A. J. R. Bourn, Y. S. Lin, *ibid.* **86**, 3576 (1964).
19. J. F. M. Oth, *Pure Appl. Chem.* **25**, 573 (1971).
20. O. Ermer, F.-G. Klärner, M. Wette, *J. Am. Chem. Soc.* **108**, 4908 (1986); L. A. Paquette, M. P. Trova, J. Luo, A. E. Clough, L. B. Anderson, *ibid.* **112**, 228 (1990); L. A. Paquette *et al.*, *ibid.*, p. 239.
21. T. J. Katz and H. L. Strauss, *J. Chem. Phys.* **32**, 1873 (1960); H. L. Strauss, T. J. Katz, G. K. Fraenkel, *J. Am. Chem. Soc.* **85**, 2360 (1963).
22. T. J. Katz, *J. Am. Chem. Soc.* **82**, 3785 (1960).
23. P. I. Kimmel and H. L. Strauss, *J. Phys. Chem.* **72**, 2813 (1968).
24. J. H. Hammons, D. A. Hrovat, W. T. Borden, *J. Am. Chem. Soc.* **113**, 4500 (1991).
25. R. Gygax, H. L. McPeters, J. I. Brauman, *ibid.* **101**, 2567 (1979).
26. W. E. Wentworth and W. Ristau, *J. Phys. Chem.* **73**, 2126 (1969).
27. M. K. Gilles, K. M. Ervin, J. Ho, W. C. Lineberger, *ibid.* **96**, 1130 (1992).
28. See, for example, J. A. Pople, M. Head-Gordon, D. J. Fox, K. Raghavachari, L. A. Curtiss, *J. Chem.*

Phys. **90**, 5622 (1989); J. A. Pople, A. P. Scott, M. W. Wong, L. Radom, *Isr. J. Chem.* **33**, 345 (1993).
29. P. Chen, in *Unimolecular and Bimolecular Reaction Dynamics*, C. Y. Ng, T. Baer, I. Powis, Eds. (Wiley, New York, 1994), pp. 371–425; P. G. Wenthold, M. L. Polak, W. C. Lineberger, *J. Phys. Chem* **100**, 6920 (1996).
30. D. A. Hrovat and W. T. Borden, unpublished results.
31. This research was supported by the National Science Foundation [grants CHE93-18639 (W.C.L.), PHY95-12150 (W.C.L.), and CHE93-14685 (W.T.B.)]. We thank R. F. Gunion and C. F. Logan for assistance with this project and J. Michl for stimulating discussions.

6 March 1996; accepted 17 April 1996

Far-Infrared Hydrogen Lasers in the Peculiar Star MWC 349A

Vladimir Strelnitski,* Michael R. Haas, Howard A. Smith, Edwin F. Erickson, Sean W. J. Colgan, David J. Hollenbach

Far-infrared hydrogen recombination lines H15α (169.4 micrometers), H12α (88.8 micrometers), and H10α (52.5 micrometers) were detected in the peculiar luminous star MWC 349A from the Kuiper Airborne Observatory. Here it is shown that at least H15α is strongly amplified, with the probable amplification factor being greater than or about equal to 10^3 and a brightness temperature that is greater than or about equal to 10^7 kelvin. The other two lines also show signs of amplification, although to a lesser degree. Beyond H10α the amplification apparently vanishes. The newly detected amplified lines fall into the laser wavelength domain. These lasers, as well as the previously detected hydrogen masers, may originate in the photoionized circumstellar disk of MWC 349A and constrain the disk's physics and structure.

Soon after the invention of the maser and laser (microwave and light amplification by the stimulated emission of radiation, respectively), natural masers with amplifications A up to 10^{12} were discovered in interstellar and circumstellar gas clouds (*1*), first at centimeter wavelengths and later in the millimeter and submillimeter domains, down to wavelengths $\lambda \approx 0.45$ mm (450 μm) (*2*, *3*). The search for natural masers (or, rather, lasers) at still shorter wavelengths is severely hampered by the opacity of our atmosphere. In fact, throughout most of the 300- to 20-μm region, ground-based observations are impossible.

Masers and lasers work on the same physical principle. In the laboratory, the distinction made between them is based on the technology used to create them, with the wavelength boundary lying roughly at several hundred micrometers (*4*). A natural dividing principle in astrophysics is the detection technology: the microwave ("wave detecting") technology used for masers and the optical ("quantum detecting") technology used for lasers. This boundary roughly coincides with that between laboratory masers and lasers and also with the above-mentioned 300-μm observational barrier.

There is no reason to doubt the existence of astrophysical lasers. For example, calculations have predicted population inversions (*5*)—a necessary condition for amplification—and, in some cases, the possibility of high gains (*6*) in the optical and near-infrared hydrogen transitions in HII regions (which are hydrogen clouds ionized by the ultraviolet radiation of nearby hot stars). Yet there is a puzzling lack of observed astrophysical lasers. In 1979, Smith *et al.* (*7*) reported an abnormally bright line at $\lambda = 4.7$ μm in the spectrum of the Becklin-Neugebauer object in Orion. The line was identified as the hydrogen Pfβ transition and, on the basis of an analysis of level populations, it was argued that it might be lasing. However, when this observation was repeated, the line was not as bright (*8*). Within the solar system, there is strong evidence for population inversions in the 10-μm CO_2 bands in the martian and venusian atmospheres (*9*). However, the predicted amplifications are very small ($A \lesssim 1.1$) and are not yet sufficient to discriminate observationally between lasing and spontaneous fluorescence. Besides, the energies involved are $\sim 10^{15}$ times smaller than the typical energies of the galactic masers. Thus, this local phenomenon is not the long-sought optical-infrared analog of the powerful, high-gain astrophysical masers.

Looking for an object that could help solve this 30-year puzzle of why astrophysical masers are observed and lasers are not, we chose MWC 349A. This luminous star, ≈30,000 $L_\odot$ (*10*), is surrounded by a massive ionized envelope that has been detected in more than 20 hydrogen emission α lines—from the visual H2α line (*11*) at 0.65 μm to the radio H92α line (*12*) at 3 cm. (Hnα denotes the hydrogen transition between the levels with principal quantum numbers n and $n + 1$.) Several of the α lines in the millimeter domain were found to have a peculiar velocity structure: two intense, narrow spectral peaks superimposed on a broad component similar to that found for other transitions (*13*). The narrowness and the high intensity of the double-peaked component have been attributed to masing (*13*). The double-peaked component first appears at H36α (2.2 mm) and is seen down to H21α (0.45 mm)—the shortest wavelength submillimeter α line observable from the ground (*2*, *13*–*16*). Yet the optical and near-infrared α lines show no sign of lasing (*17*). Thus, MWC 349A was a promising candidate for detecting the first high-gain astrophysical lasers in the far-infrared domain and for studying the transition from the apparently amplified long-wavelength lines to the apparently nonamplified short-wavelength lines. The latter could shed light on the puzzle of the lack of observed lasers in general.

We observed the H10α line at 52.5 μm on 15 June 1994 and the H12α and H15α lines at 88.8 and 169.4 μm on 16 August 1995 with the 91-cm telescope of the Kuiper Airborne Observatory (KAO), using the facility's cryogenic grating spectrometer (*18*, *19*). Spectral resolutions were ≈80, 80, and 140 km s^{-1}, respectively, and the measured fluxes were $36 \pm 13 \times 10^{-20}$, $5.5 \pm 2.5 \times 10^{-20}$, and $8.1 \pm 1.9 \times 10^{-20}$ W cm^{-2}, respectively. The H12α measurement is slightly above 2σ and is formally only an upper limit. The H10α line is measured to nearly 3σ and is a probable detection (*20*). The H15α line is more than 4σ and is clearly a solid detection (Fig. 1). The fact that all three lines are observed to fall within one-quarter channel of their expected wavelengths, which is well within our calibration uncertainty of ±0.5 channels, increases confidence in these results. No other atomic or molecular features of any significant strength are expected in any of these bandpasses.

A convincing case for lasing in the newly detected lines can be made by comparing their fluxes with those at other wavelengths and using simple phenomenological arguments concerning the nature of the emission. The nonmasing parts of MWC 349A's envelope radiate spontaneous emission in the α lines, which is partially reabsorbed by the free electrons

V. Strelnitski and H. A. Smith, Laboratory for Astrophysics, National Air and Space Museum, Smithsonian Institution, Washington, DC 20560, USA.
M. R. Haas, E. F. Erickson, D. J. Hollenbach, NASA Ames Research Center, Moffett Field, CA 94035–1000, USA.
S. W. J. Colgan, NASA Ames Research Center, Moffett Field, CA 94035–1000, and Search for Extraterrestrial Intelligence Institute, 2035 Landings Drive, Mountain View, CA 94043, USA.
*To whom correspondence should be addressed.